GIA NEWS FROM RESEARCH

The report indicates the status of a research project that is still ongoing within GIA. Comments on this and other reports and their direction are warmly welcomed as are offers of collaboration. Contact information can be found in the "about the authors" section on page 36.

A STUDY OF RUBIES FROM CAMBODIA & THAILAND

Supharart Sangsawong, Wim Vertriest, Sudarat Saeseaw & Vincent Pardieu

Figure 1: Rough and faceted rubies from Thailand-Cambodia. The rubies in matrix are associated with green pyroxene. The faceted stones in the center weigh 2.25 and 1.62 carats. Photo by Vincent Pardieu © GIA.

INTRODUCTION

Rubies in Thailand and Cambodia are found in the border area of both countries, in the areas of Pailin (Cambodia) and Chanthaburi-Bo Rai-Trat (Thailand).

Although being recovered for over 100 years, Thai and Cambodian rubies have been mined intensively in the 1960's-1990's. Those were large-scale mechanized operations. Production today has dropped drastically, but small scale and artisanal miners are still finding rubies. These are mainly on the Cambodian side of the border.

For this study, 41 samples were analyzed at the GIA laboratory in Bangkok. Internal features were documented with a focus on mineral inclusions, fingerprints and twinning planes. Advanced techniques such as UV-VIS-NIR spectroscopy were used to analyze the color of these rubies. Trace element chemistry was measured using LA-ICP-MS to support the spectroscopy and to compare this data with rubies from other deposits.

Figure 2: A map of the Thai-Cambodian border. The main ruby producing areas are inside the red circle.

Table of Contents

PART I: INTODRUCTION TO RUBIES FROM THAILAND AND CAMBODIA

History of Ruby mining in Siam

Rubies (and sapphires) are mined along the current Thai-Cambodian border for more than a century. The deposit was probably discovered during the 19th century by Burmese merchants traveling to the Mekong. Several travelers reported Burmese people searching for gems near Chanthaburi and Pailin in 1880-1896 (Smyth, 1994, Pavie, 1999).

The Pailin and Samlaut gem producing areas (Cambodia) are the continuation of the Chanthaburi-Trat mining area located in Thailand.

During most of the 19th century, at the time of the deposits discovery, the region around Chanthaburi, then known as "Chanthaboon", was under the control of the Kingdom of Siam. Following the Paknam incident in 1894, the French occupied Chanthaburi and Trat (present Thailand). These regions were returned to Siam in 1907 in exchange for the provinces of Battambang, Siem Reap and Sisophon (Present Cambodia). Pailin and Samlaut, part of the Battambang province, became part of French Indochina. After the independence in 1954, they became part of the Kingdom of Cambodia. During the war that devastated the country from 1970 to 1999, Pailin was a Khmer rouge stronghold. Pailin was declared an independent province after the civil war.

Despite the war, these deposits became an important source of rubies for the world trade during the last part of the 20th century (Lacombe, 1970, Berrangé and Jobbins, 1976, Keller 1982, Hughes 1997, 2017). Until that time, the main ruby producer was Burma (Myanmar). In 1962, the Burmese gem trade collapsed due to the military coup in the country. The international trade in Thailand was looking for a new source of rubies, particularly for smaller stones to be used as melee for their growing jewelry making industry. Thanks to the Australian mining technology, several mechanized ruby mines started in Thailand in the 1970's. The Khmer Rouge regime allowed Thai miners to work in Pailin and Samlaut to finance their fight against the Vietnamese.

Since the 1990's, the Thai ruby mines have been largely abandoned. Sporadically, some miners can be found working in the streams east of Chanthaburi towards the Thai Cambodian border. These small rivers running through plantations are worked by farmers during the dry season. The small rubies are extracted from the river gravels using very simple tools. (Hughes 1996, Pardieu 2009)

Geology of the Siamese ruby deposits

The gem deposits of Chanthaburi, Trat and Pailin are associated with alkali basalts (Keller 1982). These are basalts that form at great depths, usually assumed to be in the mantle, near the transition with the crust. SE-Asia hosts multiple alkali basalt extrusions that are of Cenozoic (Tertiary) age. Although most of them are not gem bearing or are rich enough to be commercially exploited, some of these deposits have had a serious impact on the global gemstone trade (Bo Ploi, Chanthaburi-Trat, and Pailin).

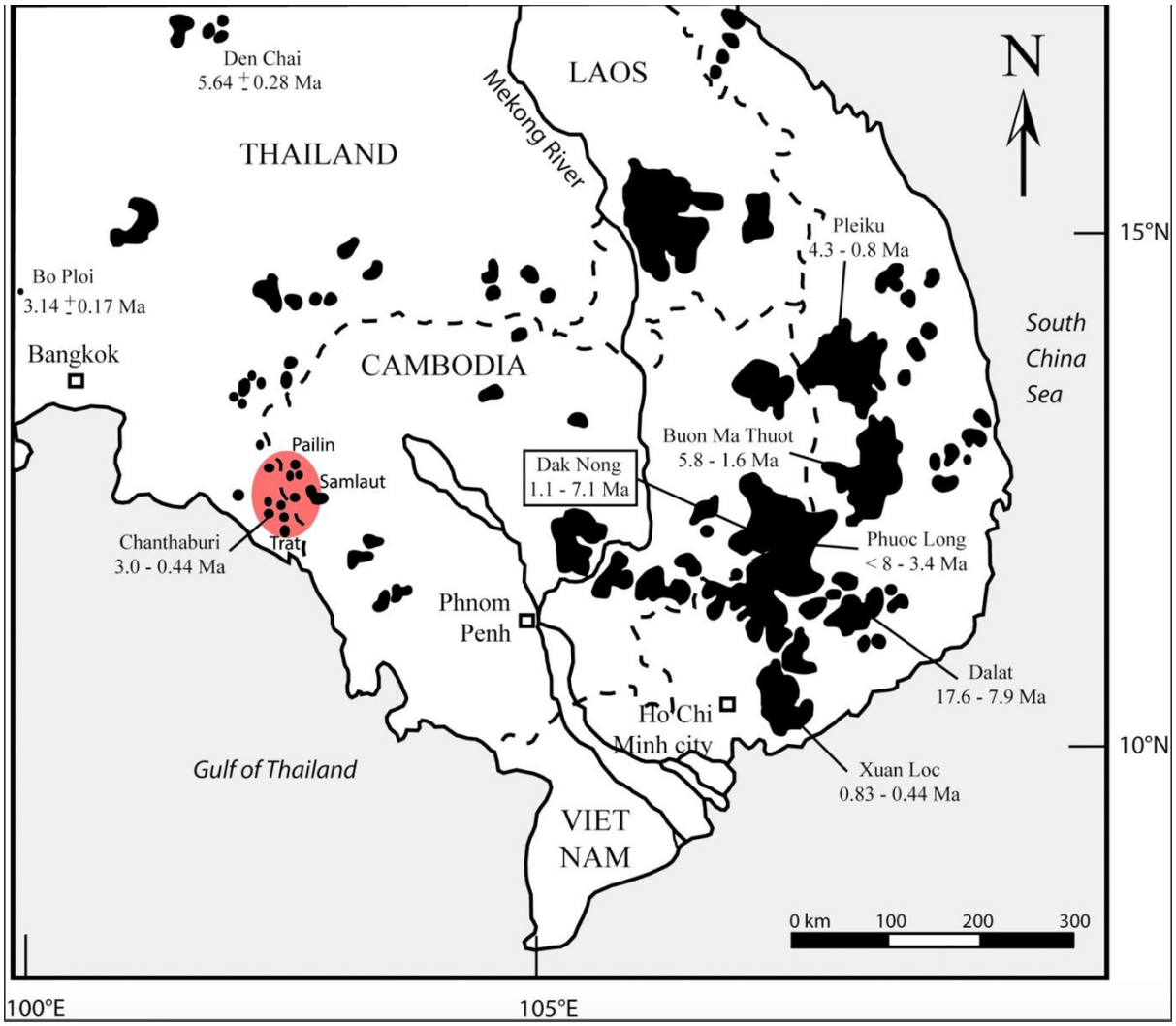

Figure 3: Map of the different basalt fields in South East Asia with their respective ages. In red is the area located along the current Thai Cambodian border where rubies are found near Chanthaburi-Trat (Thailand) and Pailin-Samlaut (Cambodia). Modified from Garnier et al, 2001

Deposits related to alkali-basalts mainly produces BGY (blue-green-yellow) sapphires, but rubies can also be found (Levinson and Cook 1994). The gems are found in these basalts as xenocrysts (Figure 4)(Levinson and Cook 1994, Sutherland 1998, Saminpanya 2011). This means that they have not formed in the basalt, but were picked up by the basalt and transported to the surface. There are several arguments for this:

- Experiments to crystallize corundum from a melt with similar composition of alkali basalt have never been successful.
- The corundum never shows a perfect crystal habit, it is always rounded (even when found in the basalt) and shows etching and resorbing, indicating the basalt has started to consume/dissolve the corundum because it is unstable in basalt surroundings.
- Several inclusions in basalt-related rubies and sapphires are impossible to form in alkali basalts.

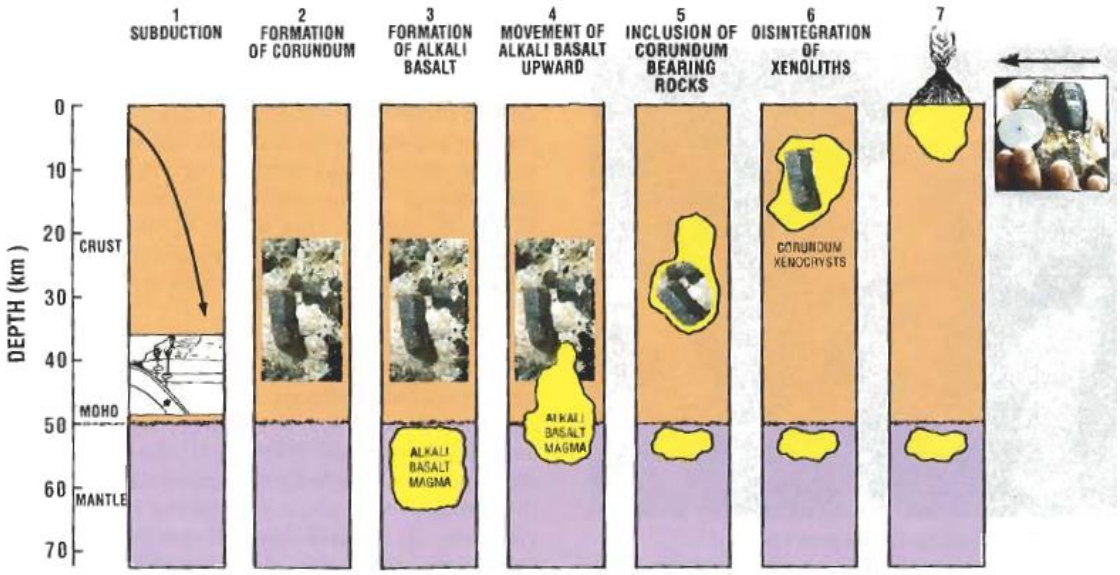

Figure 4: Visualization of the geological process behind basalt-related gem deposits (Levinson and Cook 1994).

Basaltic versus Basalt-related:

The term basaltic means that the described feature has formed in the basalt. Levinson &Cook (1994) give sufficient arguments that the ruby and sapphires found in association with basalt did not form in the basalt. Thus they are not basaltic in origin!

In the author's opinion, it is more correct to refer to these gems as **basalt-related or basalt-hosted.**

Due to South-East Asia's hot and humid climate, the alkali-basalt weathers very quickly. During the weathering process, the more stable minerals are liberated from their basalt matrix. These are mainly corundum, garnet, zircon and large clinopyroxenes. The basalt matrix, which consists of finer-grained pyroxenes, is turned into a reddish mud (Keller 1982).

The released gemstones are found in secondary, alluvial deposits. These river deposits can concentrate heavy minerals in certain locations where the river's energy and speed is locally lower. These traps are found behind large boulders, in river curves and after river-sections containing rapids.

In the river deposits around Pailin, these traps contain minerals associated with the alkali basalts, but also heavy minerals from other rocks found nearby. Examples are gold and several garnet varieties, which are also found by the miners working recent and paleo-river deposits.

Siamese versus Burmese rubies

Burmese and Siamese rubies formed in completely different geological settings. This leads to different rubies, each with their own typical inclusions suite and chemical fingerprint. The marble-related rubies from Burma have much lower Fe-content and have a very strong fluorescence. Basalt-related Siamese rubies have a very high Fe-content and consequently have very low fluorescence. Due to this higher Fe-content, the color has a more purplish aspect. To remove this purple aspect, and heal any potential fractures, rubies form Thailand and Cambodia are routinely heat-treated.

Mining techniques

Several types of ruby mining operations can be found in the area West of Pailin. The first type works in old riverbeds and operates on the largest scales. These often work with machines: including jigs, pumps and excavators. The excavators are used to remove large blocks. Pumps and high-pressure waterjets are used to loosen the finer gravels and muds. Once released, they flow towards a gravel pump. This pump transports the slurry to a mechanized jig where the heavy minerals are concentrated. At the end of the day, the jig is cleared of all valuable stones.

Figure 5: Mining old river deposits near the Pailin river. From bottom to top, we can see: Miner working high pressure waterjet to loosen the gravels; gravel pump to move the slurry; jig to concentrate the minerals. Photo by Vincent Pardieu-GIA.

Other miners work in the active riverbed. The Pailin river has strongly fluctuating levels and has its origins in the Cardamom mountains, south of Pailin. This mountainous forest hosts several alkali basalts that produce rubies and sapphires. These are transported during the rainy season. When water levels fall, many traps in the riverbed become accessible. Miners start manually washing and sieving the gravels that build up behind big boulders or in riverbends.

Figure 6: A Cambodian miner working in the Pailin river during the dry season. In the background are the Cardamom mountains, which contain several gem-hosting basalts. Photo by Wim Vertriest-GIA.

Figure 7: A miner using a long shovel to get gravel from the river bottom. Photo by Wim Vertriest-GIA.

Figure 8: A miner removing the oversized material from his washing screen. Photo by Wim Vertriest-GIA.

Some miners decided to create artificial traps by digging holes in the river bed. When the waterlevels rise, these holes trap heavy minerals. The next year, when the riverlevel has fallen again, they clean the trapped gravels.

Figure 9: Circular pits in the river, where miners have created artificial gemstone traps. Apart from mining, kids use them as swimming pools. Photo by Wim Vertriest-GIA.

PART II: MATERIALS AND METHODS

2.1 Sample Collection:

Forty-one (41) samples were selected for this study (Figure 11). 34 samples from Pailin, Cambodia and 7 samples from Chanthaburi, Thailand from GIA's reference collection were studied in depth.

The 34 rubies from Cambodia used in this study were collected by author VP while visiting active mines located around Pailin during GIA field expeditions FE04 (see: http://www.giathai.net/field-expedition-to-pailin-cambodia/), FE10, FE14, FE19, FE20, FE42 and FE47 between 2009 and 2014. Regarding the 7 Thai rubies, they were collected from a small-scale miner during the GIA Field Expedition FE07 in the Trat Province near Bo Rai on the Thai side of the border (Hughes, 2009 see: http://www.ruby-sapphire.com/thai-ruby-the-last-thai-ruby-miner.htm)

According to the GIA Field Gemology cataloguing system, these samples can be catalogued as B and C types.

- B-type: Mining was witnessed by the gemologist, usually collected from the jig.
- C-type: Sample was collected from the miner at the mine, but without witnessing the mining.

Figure 10: Author VP negotiating for gemstone samples with some river miners near Pailin, Cambodia. Photo by Wim Vertriest-GIA.

2.2 Sample fabrication:

Thirty-six (36) samples were fabricated with at least one window for inclusion photography, FTIR, and chemistry. Five (5) samples were fabricated with windows parallel to c-axis for UV-Vis-NIR spectroscopy and chemistry, Table 1. Samples were accuracy aligned either perpendicular or parallel to the c-axis by using GIA's corundum c-axis device for sample preparation (T. Thomas, 2009). Optical path lengths of the wafers were measured with a Mitutoyo series 395 spherical micrometer with an accuracy of 2 microns. Ruby samples were crystallographically oriented with the c-axis tool and then fabricated into polished wafers with the c-axis lying in the plane of the wafer. This orientation allows measurement of both O-ray and E-ray absorption spectra. The color range is from **purplish red to purple** when look down the c-axis (or parallel to the c-axis) or through a 0° wafer seeing the O-ray color (E⊥c) whereas **orangey red** is seen when one views down an a-axis (perpendicular to the c-axis) or through a 90° wafer, one is viewing a color that is 50% O-ray and 50% E-ray. Only with a dichroscope can see a pure E-ray color (E||c) as shown in Table 1.

In this study, five samples, which had differentiated characteristic mainly for Cr and Fe concentration, were selected for UV-Vis-NIR and FTIR spectroscopy (Table 1). All samples were studied for inclusions and chemistry.

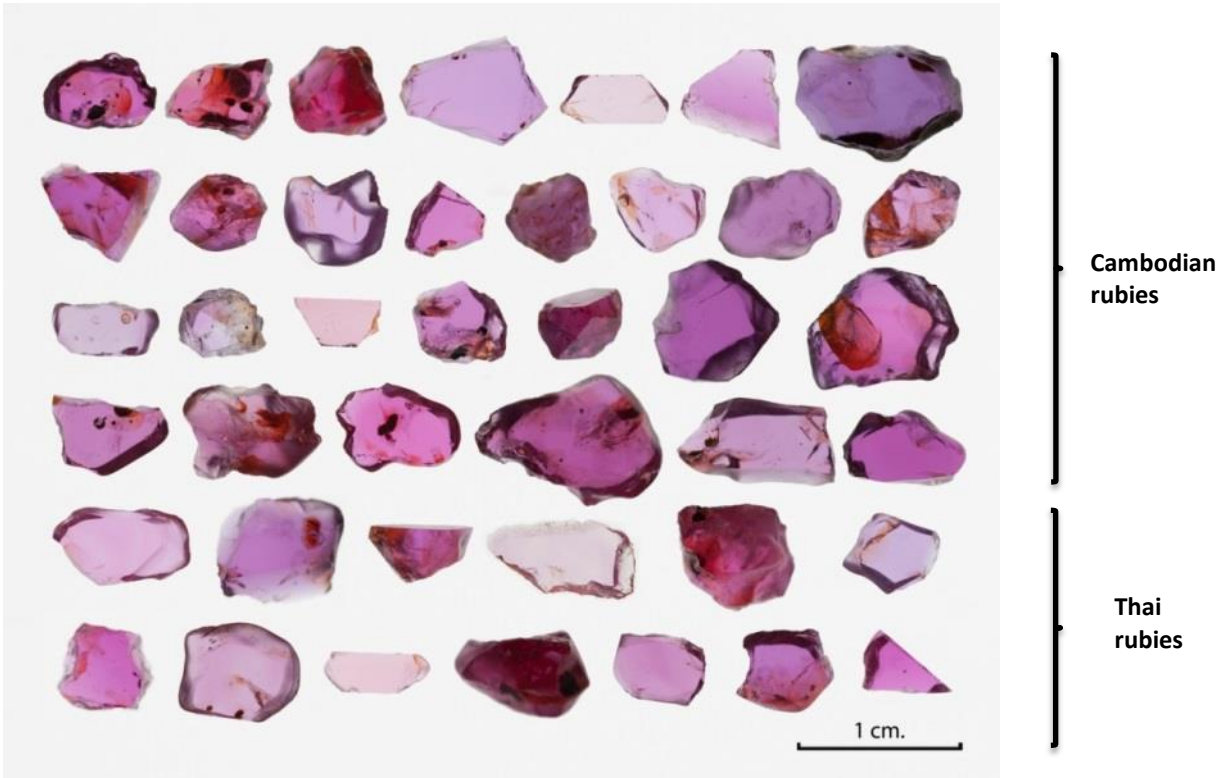

Figure 11: Polished ruby samples from Pailin, Cambodia and Chanthaburi, Thailand. The photos were color calibrated using transmitted light. Photos: S. Engniwat © GIA.

Table 1: Details of the five (5) ruby samples for UV-Vis-NIR and FTIR spectroscopy, and chemistry studies

GIA Reference #	Country	Wafer window orientation	Wafer path length (mm.)	Description* / Color:	Photo taken under Color Corrected Light Box	Photo through a dichroscope
66890**1602**	Pailin, Cambodia	90° wafer, 50% O-ray + 50% E-ray	0.644	Medium Cr / Low Fe Purplish red/Orangey red		
66883**5902**	Chanthaburi, Thailand	90° wafer, 50% O-ray + 50% E-ray	0.468	Medium to High Cr / Low Fe Purplish red/Orangey red		
100305163**677**	Pailin, Cambodia	0° wafer, 100% O-ray	0.932	Medium to High Cr / Medium Fe Purplish red		
100305163**690**	Pailin, Cambodia	0° wafer, 100% O-ray	1.563	Medium Cr / Medium Fe Purple		
100310677**107**	Pailin, Cambodia	0° wafer, 100% O-ray	0.955	Medium Cr / Low Fe Purple		

*Note: Fe concentration range; high ≥ 2500 ppma, medium = 2500-1200 ppma, low ≤ 1200 ppma
Cr concentration range; high ≥ 1300 ppma, medium = 1300-27 ppma, low ≤ 27 ppma (F.L. Sutherland ,1998)

2.3 Instrumentation:

2.3.1 SAMPLE PHOTOGRAPHY

A Canon EOS 5D camera, with a Canon Macro MP-E 65 mm lens adapted to a camera stand, was used to document the color of the samples. In order to produce consistent results for each sample, the photographs were taken under exactly the same lighting conditions, with the reference samples being placed in a Logan Electric Tru-View 810 Color Corrected Light Box (5000 K lamp). A neutral density filter was used to calibrate the camera light box combination to produce a neutral gray. High-resolution reference photographs were then collected using transmitted light. The color of the sample with polarizer aligned perpendicular to c-axis or 0° sample is the color produced by O-ray only whereas sample with polarized aligned parallel to c-axis direction or 90° sample is the color produced by O + E-ray. Photomicrographs of internal features were captured at different magnifications with a Nikon SMZ 18 system and a Nikon SMZ 1500 system using darkfield, brightfield, diffused and oblique illumination, together with a fiber-optic light source when necessary. It should be noted that magnification power of the microscope was taken into consideration when calculating the field of view (FOV) information in the captions.

2.3.2 UV-VIS-NIR SPECTROSCOPY

Ultraviolet-visible-near infrared (UV-Vis-NIR) spectra were collected with a Hitachi U-2910 spectrophotometer specially modified at GIA to include a rotatable polarizer to allow the separate collection of both the ordinary (O-) and extraordinary (E-) rays. A wavelength resolution of 1.5 nm was used. The spectra obtained were corrected by calculating the reflection loss from the index of refraction data and the data was converted to show their absorption coefficients (α,cm^{-1}) using $\alpha = 2.303A/d$, where *A* is absorbance and *d* is the path length in centimeters.

2.3.3 FOURIER TRANSFORM INFRARED ABSORPTION (FTIR) SPECTROSCOPY

FTIR spectroscopy was performed using a Thermo Nicolet 6700 FTIR spectrometer equipped with an XT-KBr beam splitter and a mercury-cadmium-telluride (MCT) detector operating with a 4× beam condenser accessory. Resolution was set at 4 cm^{-1} with 1.928 cm^{-1} data spacing. The spectra obtained were converted to be absorption coefficients (α, cm^{-1}) using $\alpha = 2.303A/d$.

2.3.4 RAMAN SPECTROSCOPY

To identify mineral inclusions, Raman spectra were obtained using a Renishaw inVia Raman microscope fitted with a 514 nm argon-ion laser. The spectra were collected in the range of 100 and 1500 cm^{-1}. The accumulation was set at a minimum of 5 until the signal to noise ratio of the spectra was adequate. The calibration was performed using the 520.5 cm^{-1} line of a silicon wafer. In all cases, the RRUFF database was used as a reference when identifying inclusions. Spectral comparisons were performed using Renishaw Wire (version 3.4) and/or Thermo Galactic 'Spectra ID' (version 3.02) software.

2.3.5 LASER ABLATION-INDUCTIVELY COUPLED PLASMA-MASS SPECTROMETRY (LA-ICP-MS)

Chemical analysis was carried out using LA-ICP-MS technology with a Thermo Fisher Scientific iCAP Q Induced Coupled Plasma-Mass Spectrometer (ICP-MS) coupled with a Q-switched Nd:YAG Laser Ablation (LA) device operating at a wavelength of 213 nm. Laser conditions used were 55 μm diameter laser spots, a fluency of around 10 J/cm^2, and a 15 Hz repetition rate. Twelve spots were analyzed on each wafer. ICP-MS was operated using the forward power at ~ 1350 W and the typical nebulizer gas flow at ~ 1.00 L/min. Helium was used as the carrier gas in the laser ablation unit and the flow rate was set at ~ 0.60 L/min. The criteria for the alignment and tuning sequence were to maximize Be counts and to keep the ThO/Th ratio below 2%. A special set of doped synthetic corundum standards including Be, Mg, Ti, V, Cr, Fe, and Ga were used for quantitative analysis. All elemental measurements were normalized to Al as the internal elemental standard, (Al=529,200 ppmw or 52.92 wt.%). This value approximates to the chemical composition of corundum.

PART III: RESULTS AND DISCUSSION

Cambodia-Thai rubies have red to purplish red color. Standard gemological properties were as expected for natural ruby:

- RI= 1.760±0.002 to 1.770±0.002
- Ruby absorption spectrum seen in handheld spectroscope.
- Their fluorescence was weak to medium red under long-wave and inert under short-wave lighting.

3.1 The internal world of rubies from Cambodia/Thailand

Characteristic inclusions in rubies from the Cambodia-Thai border are mineral inclusions (such as diopside, negative crystals, and etc.) surrounded with fluid fingerprints or thin film, natural healed fractures, and intersecting polysynthetic twinning planes with growth tubules. The following photos focus deeper on these types of inclusions.

3.1.1 DIFFERENT MINERAL INCLUSIONS OR NEGATIVE CRYSTALS, AND SOME CRYSTALS ACCOMPANIED BY 'ATOLL-LIKE' FLUID FINGERPRINTS OR THIN FILMS

Figure 12: Thin films in GIA reference sample 668835502. Fiber-optic light illumination. FOV 1.2 mm. Photo: J. Muyal © GIA.

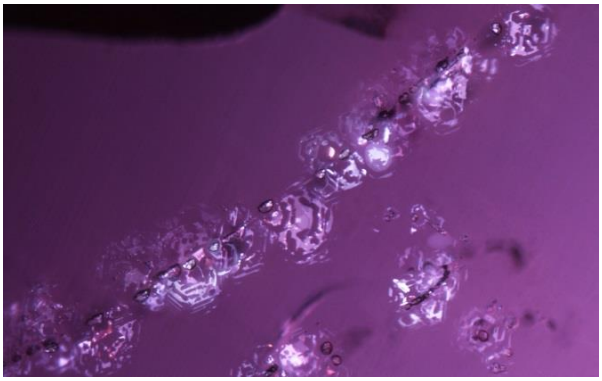

Figure 13: Unknown crystals associated with fluid fingerprints oriented in a basal plane in GIA reference sample 669321702. Darkfield with fiber-optic light illumination. FOV 1.7 mm. Photo: J. Muyal © GIA.

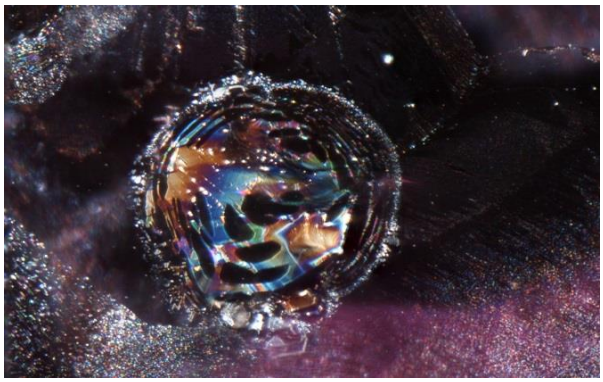

Figure 14: Fluid fingerprint in GIA reference sample 100305163702. Fiber-optic light illumination. FOV 1.1 mm. Photo: J. Muyal © GIA.

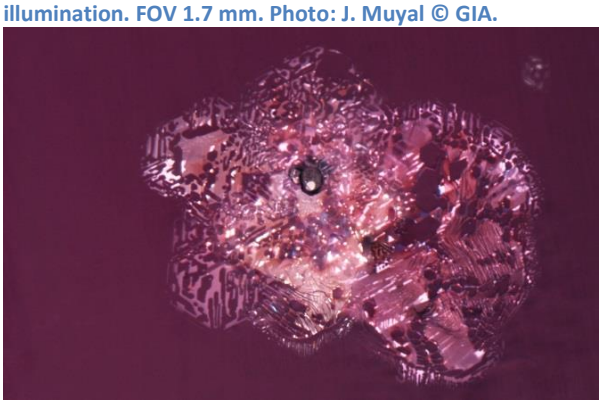

Figure 15: Unknown crystal associated with fluid fingerprint in GIA reference sample 668901802. Fiber-optic light illumination. FOV 1.7 mm. Photo: J. Muyal © GIA.

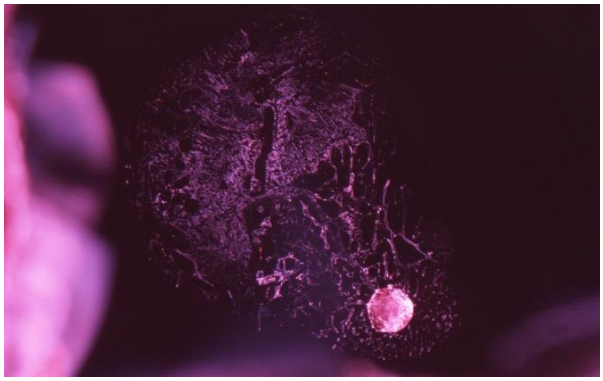

Figure 16: Unidentified frosted crystal inclusion with fluid fingerprint in GIA reference sample 668835902. Darkfield illumination. FOV 1.7 mm. Photo: J. Muyal © GIA.

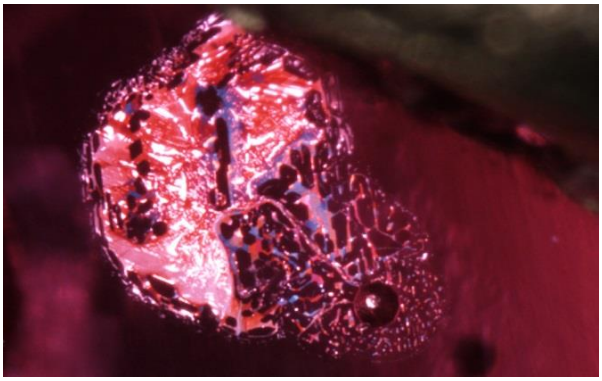

Figure 17: Using a different lighting technique on the inclusion from Figure 16 puts the focus on different aspects of this inclusion. Darkfield with fiber-optic light illumination. FOV 1.7 mm. Photo: J. Muyal © GIA.

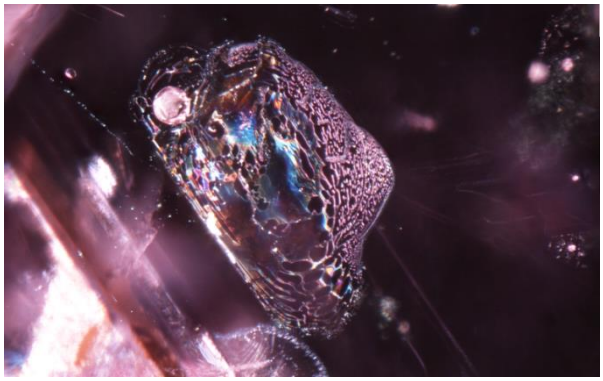

Figure 18: Molten crystal with a frosted appearance associated with fluid fingerprint in GIA reference sample 100305163690. Darkfield with fiber-optic light illumination. FOV 1.4 mm. Photo: J. Muyal © GIA.

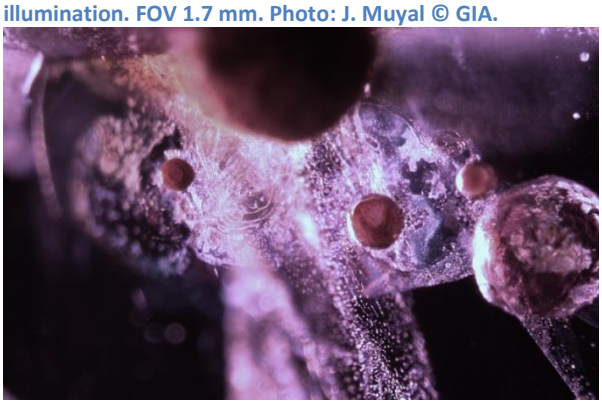

Figure 19: Unidentified orangey brown crystals associated with fluid fingerprint in GIA reference sample 100305163677. Darkfield with fiber-optic light illumination. FOV 1.5 mm. Photo: T. Bhusrisom © GIA.

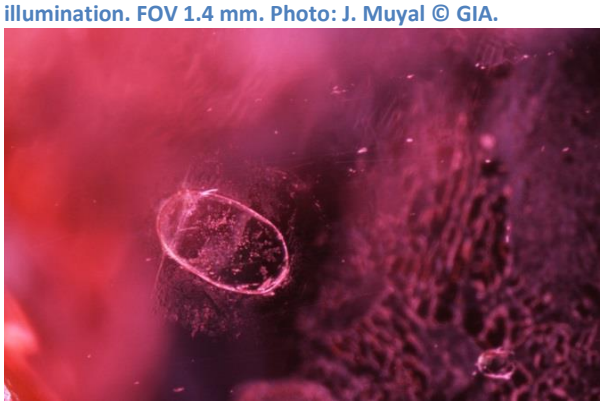

Figure 20: Oval crystal (identified as diopside by Raman using the RRUFF database as a reference) in GIA reference sample 668835502. Darkfield illumination. FOV 1.5 mm. Photo: J. Muyal © GIA.

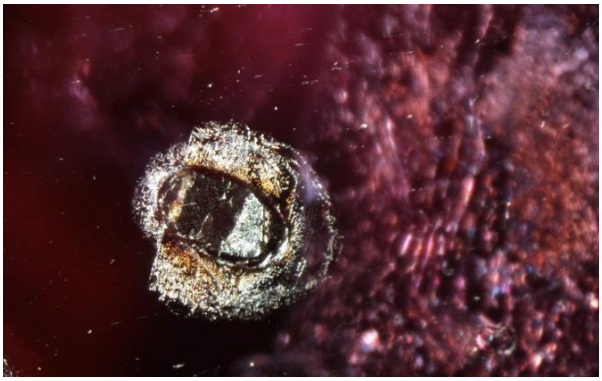

Figure 21: Using darkfield and fiber optic illumination, diopside with decrepitation halo in GIA reference sample 668835502. FOV 1.5 mm. Photo: J. Muyal © GIA.

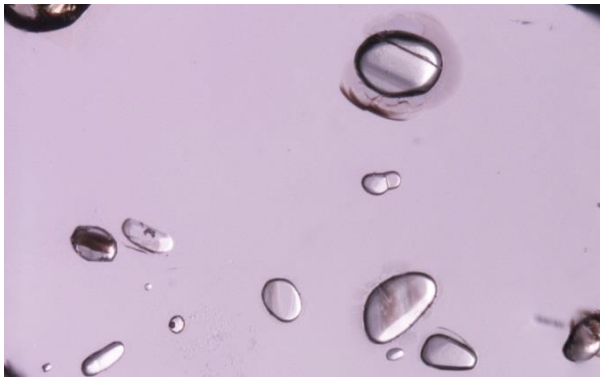

Figure 22: Multiple rounded crystals (diopside identified by Raman using the RRUFF database as a reference) in GIA reference sample 668922502. Brightfield illumination. FOV 2.0 mm. Photo: J. Muyal © GIA.

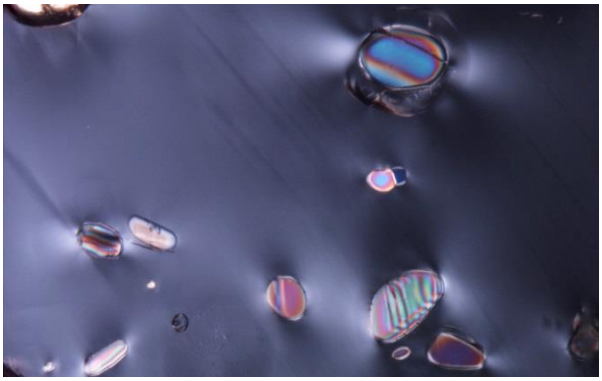

Figure 23: Between crossed polars, interference colors are seen in various diopside crystals in GIA reference sample 668922502. FOV 2.0 mm. Photo: J. Muyal © GIA.

Figure 24: Two phase fluid films Fluid inclusions containing a single gas bubble (CO_2 identified by Raman using the RRUFF database as a reference) in GIA reference sample 668917202. Darkfield illumination. FOV 1.2 mm. Photo: V. Raynaud © GIA.

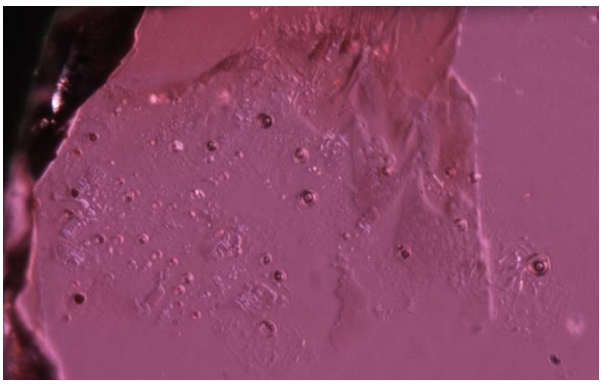

Figure 25: Two phase fluid films contained a single bubble (CO_2 identified by Raman using the RRUFF database as a reference) in GIA reference sample 668917202. Brightfield illumination. FOV 1.2 mm. Photo: V. Raynaud © GIA.

3.1.2 NATURAL HEALED FINGERPRINTS

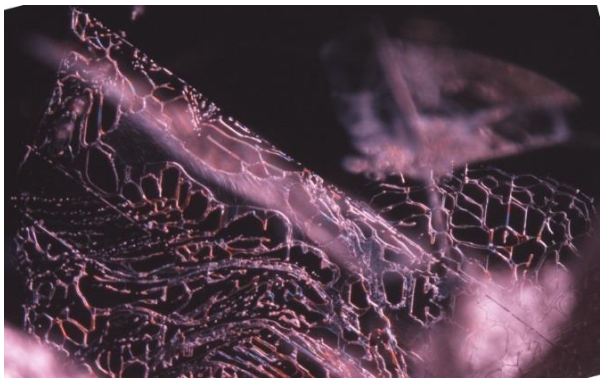

Figure 26: Naturally healed fissures in GIA reference sample 668917802. Darkfield illumination with shadowing technique. FOV 2.0 mm. Photo: J. Muyal © GIA.

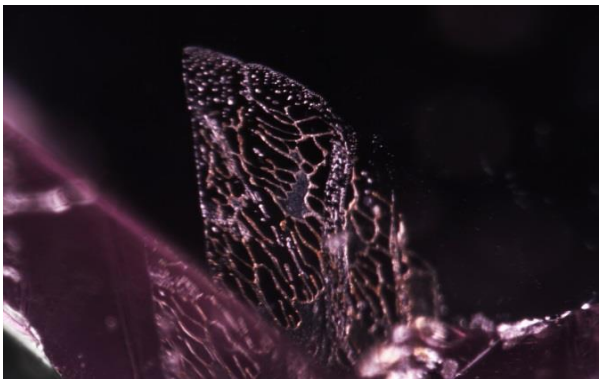

Figure 27: Naturally healed fissures in GIA reference sample 100310677107. Darkfield and fiber-optic illumination. FOV 1.05 mm. Photo: S. Sangsawong © GIA.

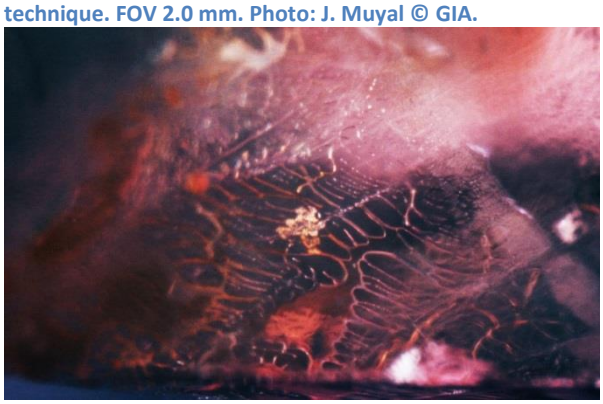

Figure 28: Fingerprint associated with iron stain in GIA reference sample 100305163693. Darkfield illumination. FOV 1.5 mm. Photo: J. Muyal © GIA.

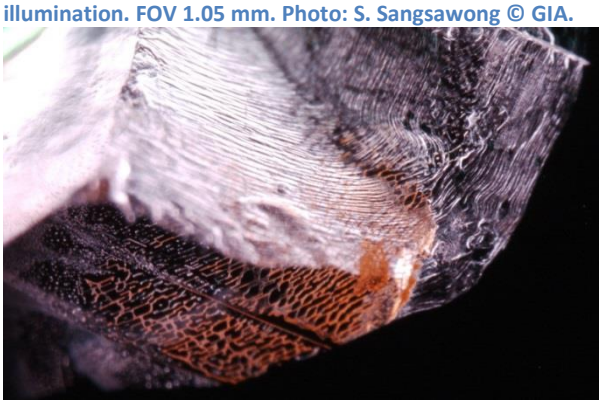

Figure 29: Fingerprint associated with orange iron stains in GIA reference sample 100305163693. Darkfield illumination. FOV 2.0 mm. Photo: J. Muyal © GIA.

Figure 30: Partially healed fractures associated with iron stains and cloudy materials in GIA reference sample 669321802. Brightfield illumination. FOV 1.3 mm. Photo: J. Muyal © GIA.

Figure 31: Epigenetic materials (boehmite and kaolinite identified by FTIR spectroscopy) in GIA reference sample 100305163680. Brightfield illumination. FOV 1.1 mm. Photo: J. Muyal © GIA.

3.1.3 POLYSYNTHETIC TWINNING WITH INTERSECTING GROWTH TUBULES

Figure 32: Intersecting lamellar twinning associated with growth tubules in GIA reference sample 100305163702. Brightfield illumination with cross polarized filter. FOV 1.2 mm. Photo: C. Khowpong © GIA.

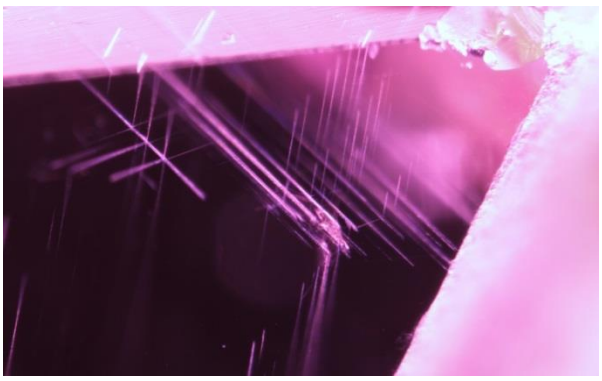

Figure 33: Same as figure 32, under brightfield illumination without cross polarized filter. FOV 1.2 mm. Photo: C. Khowpong © GIA.

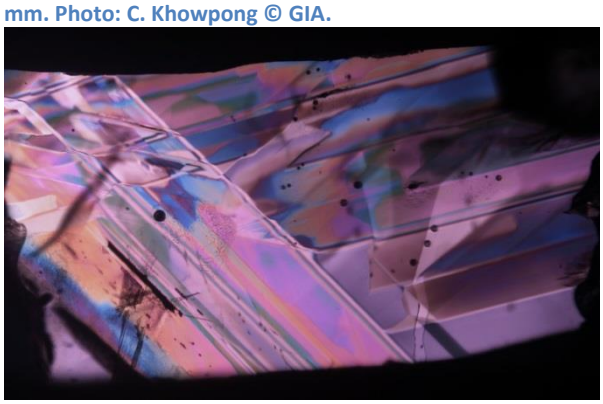

Figure 34 Lamellar twinning in three directions in GIA reference sample 100305163690. Brightfield illumination with cross polarized filter. FOV 4.8 mm. Photo: S. Sangsawong © GIA.

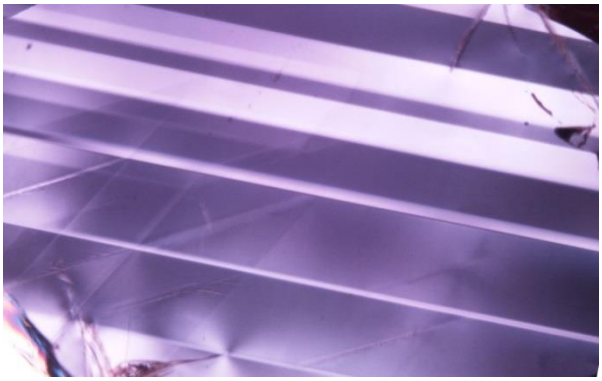

Figure 35: Polysynthetic twinning parallel to the rhombohedron in plane-polarized light in GIA reference sample 668837202. Fiber-optic light illumination. FOV 3.1 mm. Photo: J. Muyal © GIA.

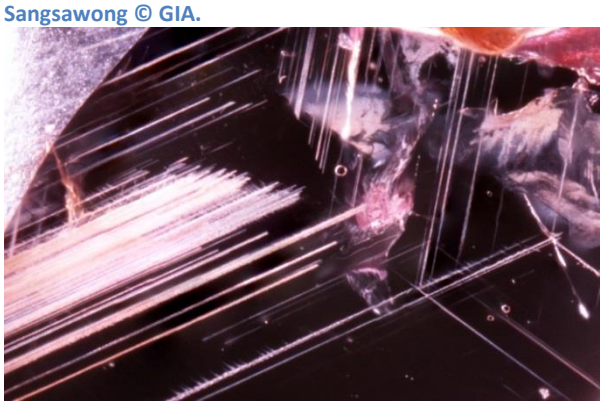

Figure 36:Parallel and intersecting growth tubules in GIA reference sample 668917702. Darkfield illumination. FOV 2.8 mm. Photo: J. Muyal © GIA.

Figure 37: Angular and intersecting growth tubules in GIA reference sample 100305163702. Darkfield illumination. FOV 1.3 mm. Photo: J. Muyal © GIA.

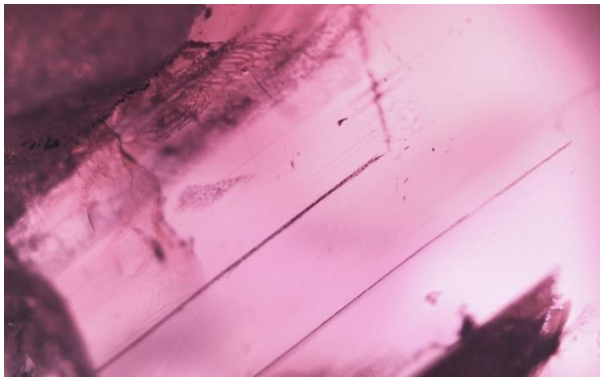

Figure 38: Growth tubules in GIA reference sample 100310677106. Brightfield illumination. FOV 1.2 mm. Photo: V. Raynaud © GIA.

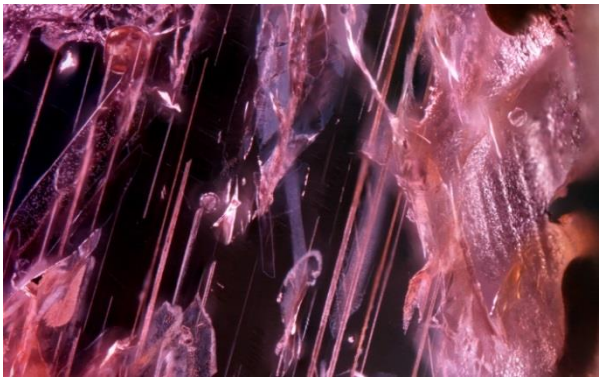

Figure 39:Parallel growth tubules filled with iron stains in GIA reference sample 668917602. Darkfield illumination. FOV 2.5 mm. Photo: J. Muyal © GIA.

3.2 Spectroscopy and chemistry of rubies from Thailand and Cambodia

3.2.1 UV-VIS-NIR SPECTROSCOPY AND CHEMICAL ANALYSIS

UV-Vis-NIR spectra of Cambodia-Thai rubies reveal the presence of Fe^{3+} and Cr^{3+} chromophores which are related to the red color of ruby Other present chromophores are Fe^{2+}-Ti^{4+} pair that create a blue color. The combination of these chromophores results in a purplish red. The details of each chromophore are below (Powell, 1998; Ferguson, 1971; and Hughes, 2017; chapter 4; Moon, A.R. and Phillips, M.R. (1994))

Cr^{3+} features

- A weak narrow line at about 694 nm termed as R-line. In reality, the R-line is two weak lines, assigned as R1 and R2, which are separated by 1.4 nm. However, our instrument resolution is 1.5 nm and we view this as a single line. The weak lines near 660 nm and 470 nm are called the S-lines and B-lines, respectively.
- A broad band at about 547-560 nm termed as U band
- A broad band at about 397-412 nm termed as Y band

Fe^{3+} or/and Fe^{2+} charge transfer with Ti^{4+} or (Fe^{2+}-Ti^{4+}) features

- The bands at 330, 377, 450, and 540 nm are due to Fe^{3+} - Fe^{3+} pairs
- The band at 388 nm is a single Fe^{3+}
- The broad iron bands at 700 and 1050 nm ~~h~~ave not been ascribed to single ions or pairs. They are quite weak except at high iron concentrations.
- The broad band of ordinary ray (O-ray) at 580 nm is assigned to Fe^{2+}-Ti^{4+} charge transfer. This absorption is concealed under (or hidden by) the U-band or Cr^{3+} band at 560 nm. To see Fe^{2+}-Ti^{4+} absorption, the Cr^{3+} spectrum needs to be subtracted out, see figure 45.

Two samples, GIA reference sample #1602 and #5902 are represented by UV-Vis-NIR spectra in this study, figure 40 and 42. Chemistry data reported on each spectrum which collected in the same area on each side of wafers, total 12 spots, figure 41, 43 and table 2, 3.

GIA reference sample #1602-ruby from Cambodia

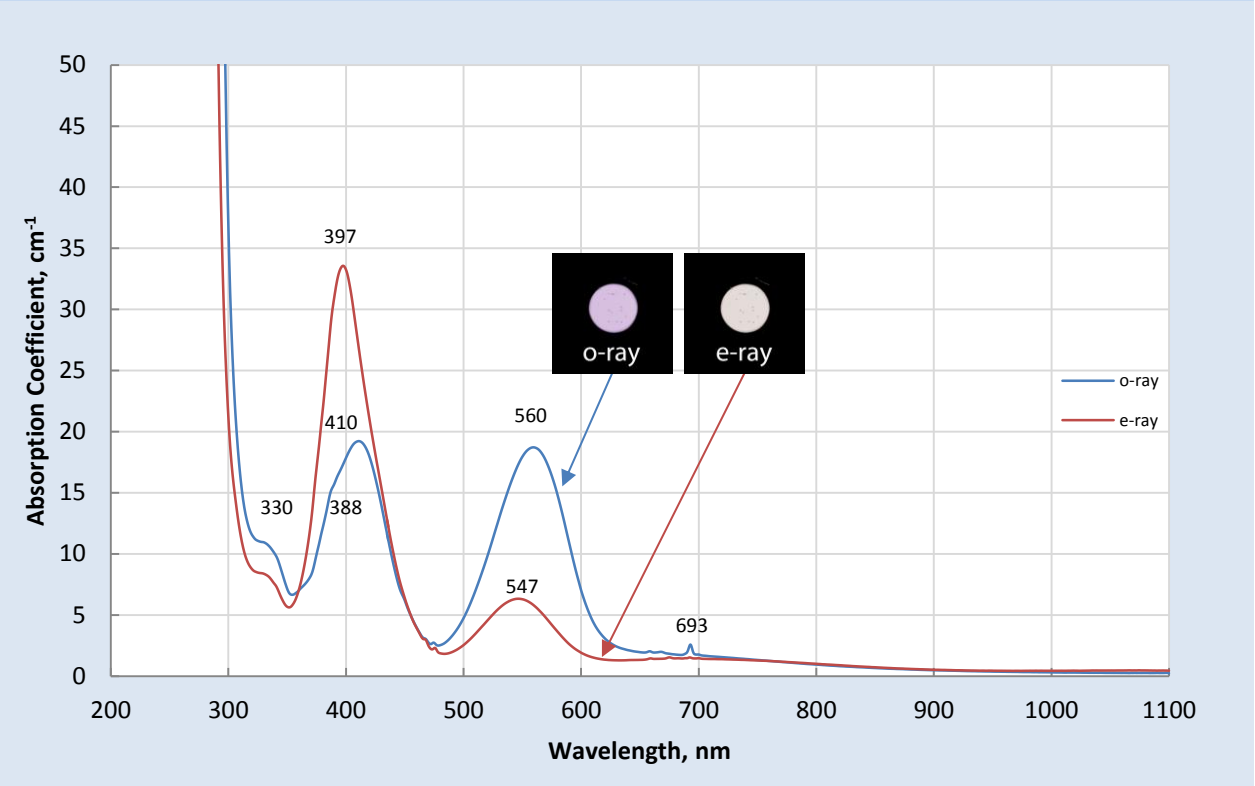

Figure 40: Polarized UV-Vis-NIR absorption spectra of GIA reference specimen #1602 with inset color calibrated polarized photos of the beam path area for the O- and E-rays. Optical path length: 0.644 mm. Color: orangey red.

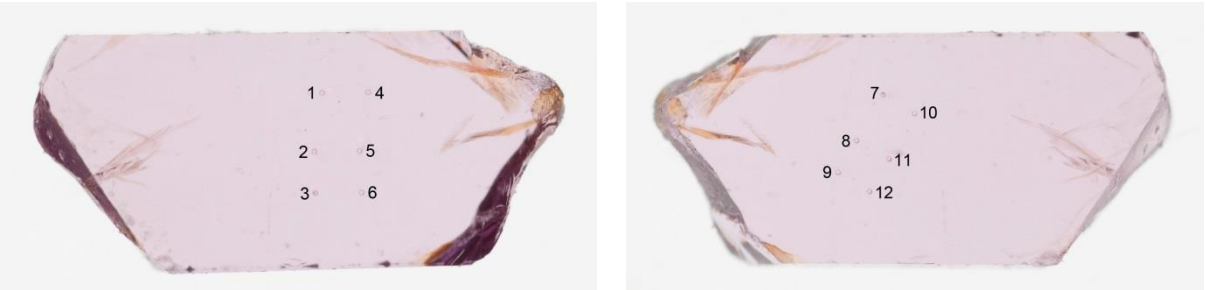

Figure 41: GIA reference sample #1602 showing the location of the 12 spots where LA-ICP-MS analysis was conducted on each side of the wafer. Photo: S. Engniwat © GIA.

Table 2: LA-ICP-MS results in parts per million atomic (ppma) units for GIA reference sample #1602. "BDL" stands for "Below Detection Limit", "BQL" stands for "Below Quantification Limit"

GIA Ref Sample #1602 (color of the area)	Concentration in ppma							
	^{9}Be	^{24}Mg	^{47}Ti	^{51}V	^{53}Cr	^{57}Fe	^{60}Ni	^{69}Ga
SP1 (orangey red)	BDL	179	94	14	780	891	4	10
SP2 (orangey red)	0.4	182	90	14	780	938	4	9
SP3 (orangey red)	BDL	188	98	14	773	920	4	9
SP4 (orangey red)	BDL	165	96	14	776	891	5	10
SP5 (orangey red)	BDL	164	89	14	788	880	4	9
SP6 (orangey red)	BDL	169	93	15	776	898	4	10
SP7 (orangey red)	BDL	164	89	14	753	884	3	9
SP8 (orangey red)	BDL	158	86	14	741	818	3	9
SP9 (orangey red)	BDL	161	80	14	749	825	4	9
SP10 (orangey red)	0.3	159	92	14	773	949	4	10
SP11 (orangey red)	BDL	160	89	14	784	924	3	9
SP12 (orangey red)	BDL	166	91	14	745	887	4	9
Average±SD		**168±10**	**91±5**	**14±0.3**	**768±16**	**892±40**	**4±0.4**	**9±0.4**
Detection limit	**0.09**	**0.1**	**0.6**	**0.1**	**0.9**	**6**	**0.03**	**0.05**

GIA reference sample #5902-ruby from Cambodia

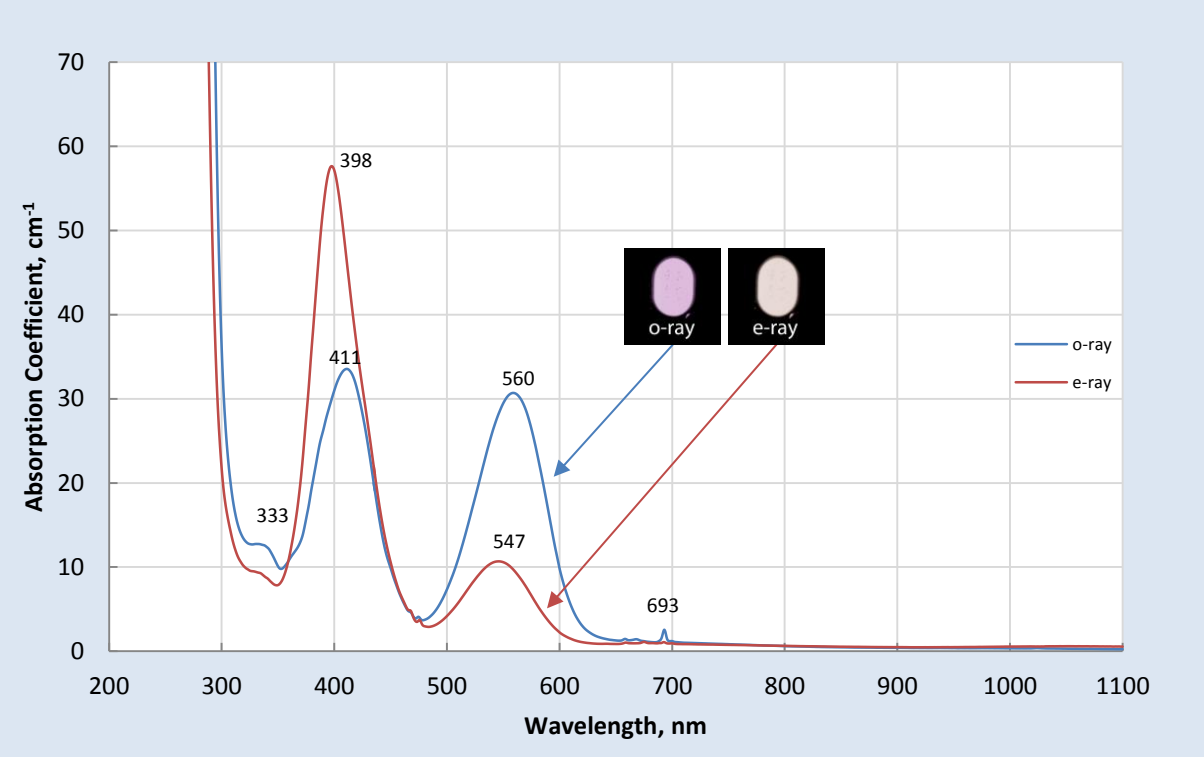

Figure 42: Polarized UV-Vis-NIR absorption spectra of GIA reference specimen #5902 with inset color calibrated polarized photos of the beam path area for the o- and e-rays. Optical path length: 0.468 mm. Weight: 0.080 carats. Color: orangey red.

Figure 43: GIA reference sample #5902 showing the location of the 12 spots where LA-ICP-MS analysis was conducted on each side of the wafer. Photo: S. Engniwat © GIA.

Table 3: LA-ICP-MS results in parts per million atomic (ppma) units for GIA reference sample #5902.

GIA Ref Sample #5902 (color of the area)	Concentration in ppma							
	^{9}Be	^{24}Mg	^{47}Ti	^{51}V	^{53}Cr	^{57}Fe	^{60}Ni	^{69}Ga
SP1 (orangey red)	BDL	126	41	5	1345	763	3	8
SP2 (orangey red)	BDL	133	43	5	1349	759	3	7
SP3 (orangey red)	BDL	135	40	6	1384	814	3	8
SP4 (orangey red))	BDL	129	44	5	1416	774	3	7
SP5 (orangey red)	BDL	131	41	6	1463	770	3	7
SP6 (orangey red)	BDL	132	41	5	1514	756	3	7
SP7 (orangey red)	BDL	142	41	6	1384	796	3	7
SP8 (orangey red)	BDL	133	39	5	1345	759	3	7
SP9 (orangey red)	BDL	136	40	6	1412	800	3	7
SP10 (orangey red)	BDL	135	42	5	1369	803	3	8
SP11 (orangey red)	BDL	141	45	5	1376	811	3	7
SP12 (orangey red)	BDL	141	47	5	1333	807	3	7
Average±SD		**134±5**	**42±2**	**5±0.2**	**1391±53**	**784±23**	**3±0.2**	**7±0.3**
Detection limit	**0.04**	**0.06**	**0.5**	**0.08**	**0.7**	**4**	**0.03**	**0.04**

Comparison of UV-Vis-NIR spectrum (O-ray) for GIA reference #3677, #3690, and #7107

The o-ray of three studies samples; GIA reference number #3677, #3690, and #7107, were shown the main characteristic absorption of Cambodian-Thai rubies border line region, figure 44. These samples were selected due to their differences in Cr and Fe chromophores giving differences in UV-Vis-NIR spectra.

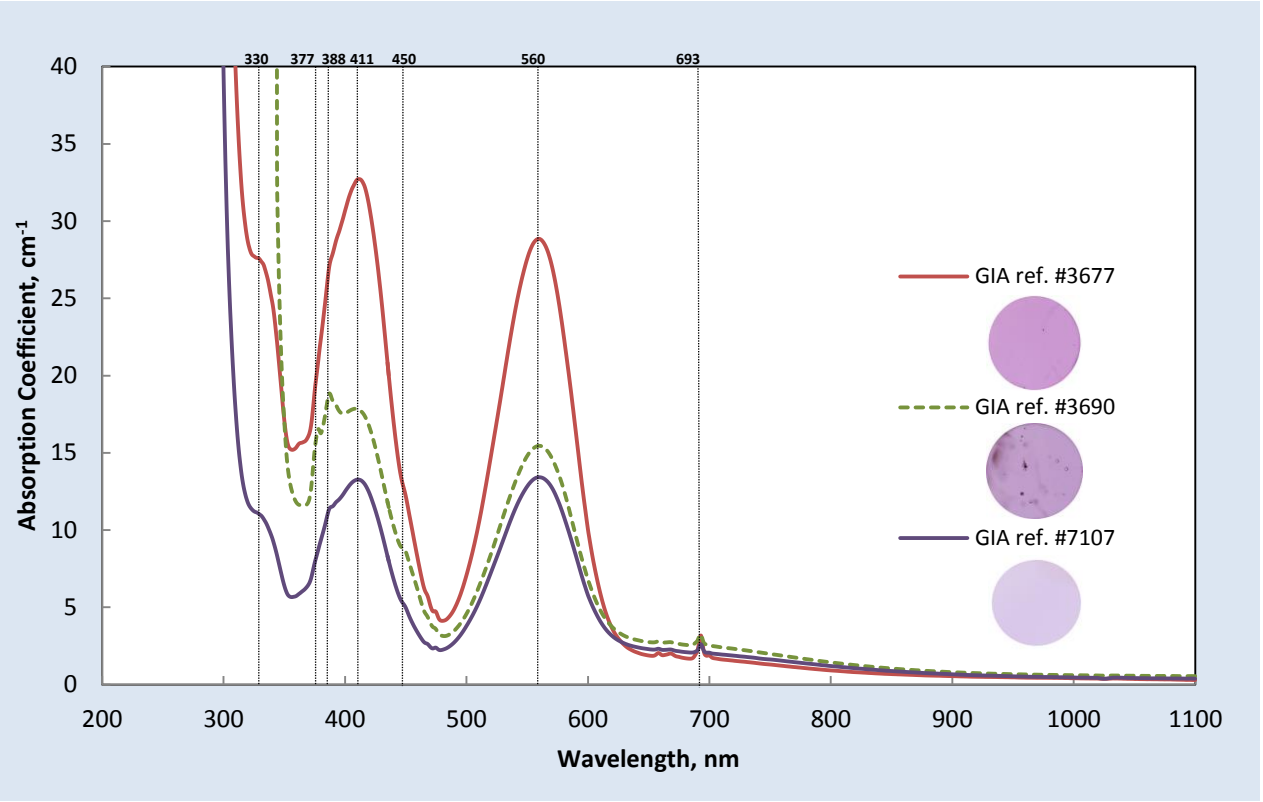

Figure 44: UV-Vis-NIR absorption spectra and average elemental concentration of GIA reference number #3677, #3690, and #7107. Optical path length: 0.932, 1.563, and 0.955 mm, respectively.

Table 4: Comparison LA-ICP-MS results in GIA reference samples #3677, #3690, and #7107.

GIA Reference Sample (Color of the area)	Concentration in ppma (Average±SD)						
	^{24}Mg	^{47}Ti	^{51}V	^{53}Cr	^{57}Fe	^{60}Ni	^{69}Ga
#3690 (Purplish red)	136±3	79±6	9±1	577±28	1868±76	2±0.2	9±0.4
#3677 (Purplish red)	135±7	52±2	12±1	1265±43	1612±133	2±0.4	7±0.4
#7107 (Purplish red)	181±4	104±4	11±1	521±34	987±24	3±0.4	9±0.3
Detection limit	*0.06*	*0.5*	*0.08*	*0.9*	*4*	*0.03*	*0.04*

GIA reference sample #3677 contained Cr (1265 ppma) with Fe (1612 ppma), which produced a purplish red color. The sample presented a Cr spectrum, with peaks at 411, 560, and 693 nm – in combination with an Fe spectrum, which can only be seen as a shoulder at 330 nm and peak at 388 nm. Both of these features are related to single Fe^{3+}.

GIA reference sample #3690 with Cr (577 ppma) and Fe (1868 ppma), had less reddish color. The absorption spectrum showed Cr and Fe spectrum with dominant peak at 377, 388, and 450 nm. Note that there was no shoulder observed in this sample due to high Fe concentration.

GIA reference sample #7107 with Cr (521 ppma) and Fe (987 ppma), shows some Fe spectrum characteristics. These can be seen as an absorption shoulder at 330 nm, and a peak at 388 nm, which is assigned to single Fe^{3+}. Features at 377 and 450 nm, normally assigned to absorptions by Fe^{3+}-Fe^{3+} pairs, were hard to observe due to low Fe content.

Most Cambodian-Thai rubies show a combination spectrum of Cr^{3+} (red color) and Fe^{2+}-Ti^{4+} pairs (blue color) giving a purple color. The features caused by Fe^{2+}-Ti^{4+} pairs at 580 nm are hidden under the U-band at 560 nm which is caused by Cr. If the Cr spectrum is subtracted from this ruby's spectrum, we can see the remaining features. For example, GIA reference sample #3690 clearly shows Fe^{2+}-Ti^{4+} pairs at about 580 nm, and Fe^{3+} at 377, 388, and 450 nm, when the Cr spectrum is removed. (See dotted line in figure 45.)

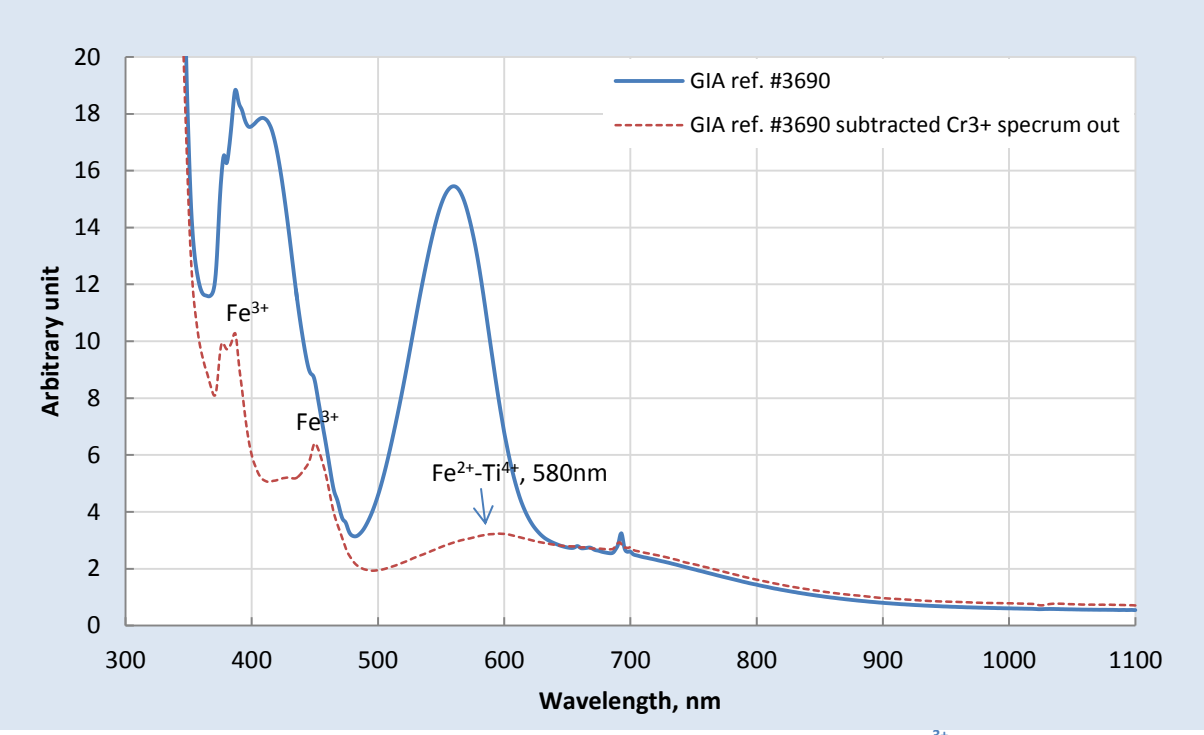

Figure 45: Overlay spectrum of GIA reference sample #3690 –blue line and after subtracted Cr^{3+} spectrum out – red line.

Cambodia-Thai rubies have noticeably higher Mg than Ti concentrations, which is uncommon for natural corundum. In theory, if Mg charge compensates Ti completely, Fe^{2+} and Ti^{4+} cannot pair to create a blue hue. However, Cambodian-Thai rubies often have a purplish tint which doesn't correspond to their Ti and Mg content. As a result, we analyzed sample #7107's chemistry using SIMS. The results showed no significant difference between SIMS and earlier LA-ICP-MS analysis. However, SIMS analysis has the advantage that it is able to detect Si. The Si content in sample #7107 averages 104 ppma (table 5). As Si is the highest-lying donor, it pairs with Mg first. After that, Mg will pair with Ti, and any excess Ti will pair to Fe producing the blue color (Emmett, 2017). In GIA reference sample #7107, Si^{4+} will pair with Mg first, thus, available Mg^{2+} will be at 43 ppma. Then Ti^{4+} will pair with available Mg^{2+}. Excess Ti^{4+} at 53 ppma will pair with Fe^{2+}, producing a blue coloration, which results in the ruby's purplish red hue. However, Fe^{2+}-Ti^{4+} pairs at this concentration, (53

ppma), create dark blue which contrasts with the purplish red observed. Currently, we cannot explain why and further study is required.'

Table 5: SIMS results in parts per million atomic (ppma) units for GIA reference sample #7107. SD is standard deviation from 5 spots analysis.

GIA Ref Sample #7107 (color of the area)	Concentration in ppma								
	Mg	**Si**	**Mg-Si**	**Ti**	**Ti-(Mg-Si)**	**V**	**Cr**	**Fe**	**Ga**
SP1 (Purplish red)	201	141	61	95	35	10	555	1043	11
SP2 (Purplish red)	184	162	23	94	72	9	513	961	9
SP3 (Purplish red)	193	152	41	97	56	9	539	1022	10
SP4 (Purplish red)	193	148	45	96	51	10	529	1025	10
SP5 (Purplish red)	194	147	48	97	49	10	526	1029	10
Average±SD	**191±6**	**104±4**	**43±14**	**96±1**	**53±13**	**10±0.1**	**533±16**	**1016±32**	**10±0.5**
Detection limit	*<0.1*	*<0.1*		*<0.1*		*<0.1*	*<0.1*	*<0.1*	*<0.1*

3.2.2 FOURIER TRANSFORM INFRARED SPECTROSCOPY OR FTIR

Infrared spectra were collected through the same area used to collect the UV-Vi-NIR spectrum. Five (5) studied samples were not observed any useful signal or no diagnostic features in the region of interest (2800-3500 cm^{-1}), figure 46. FTIR spectra obtained from Cambodian-Thai rubies show four main features:

1. Without FTIR feature peaks –most often occurred in Cambodia-Thai rubies
2. Kaolinite mineral features
3. 3309 cm^{-1} - the FTIR absorption peak at 3309 cm^{-1} is observed 15% in this study with a very weak to weak absorption.

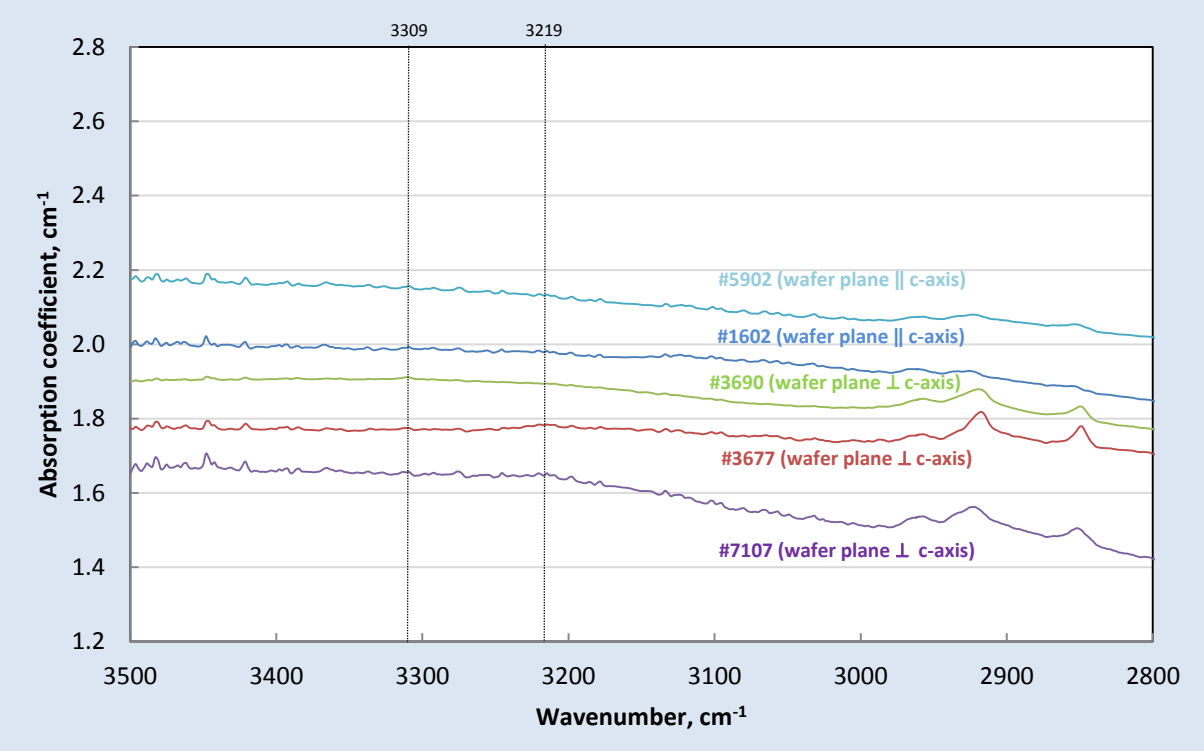

Figure 46: Un-oriented FTIR spectra of GIA reference sample #1602, #3677, #3690, #7107, and #5902 in the 2800 to 3500 cm^{-1} range. Optical path length: a) 0.166; b) 0.234; c) 0.058 and d) 3.49 mm.
*** Without the polarizer in the FTIR spectrometer, it wasn't possible to obtain accurate optical FTIR spectra.**

3.3 Comparison between Cambodian-Thai rubies and other high iron rubies based on chemistry

Generally speaking, rubies are found in three geological settings. Two of those have a tendency to form high Fe rubies: amphibole-related and basalt-related. Marble-related rubies have much lower Fe concentrations. Each geological setting also results in a different inclusion set. This means that in general the inclusion suite of basalt-related rubies is different from the inclusions found in amphibole-related rubies.

Rubies from Cambodian-Thai border region show significant trace elements, magnesium (Mg), titanium (Ti), vanadium (V), chromium (Cr), iron (Fe), nickel (Ni), and gallium (Ga). High concentration of Mg was detected at 154 and 143 ppma for Cambodia and Thai rubies respectively. Average Fe concentration was 1317 ppma for Pailin, Cambodia and 1089 ppma for Thailand. Also remarkable is that all samples showed significant Ni up to 7 ppma.

The results of rubies from Cambodian-Thai border region (number of samples, n = 34 for Cambodian and n= 7 for Thai rubies) were compared with other high iron (Fe) rubies from the GIA database (Table 6), including amphibole related rubies from Montepuez; Mozambique (n = 99), Winza; Tanzania (n = 14), Zahamena (n = 66), Andilamena (n = 14), and Vatomandry (n = 3) ; Madagascar and basalt-related rubies from Baringo, Kenya (n = 20). Low Fe-rubies are not included because they can be easily discriminated based on Fe content. Low Fe ruby (marble-related) sources include Myanmar, Vietnam and Afghanistan. We consider rubies with an average Fe concentration higher than 300 ppma, as high Fe rubies.

The most useful plotting to separate Cambodian-Thai rubies from others is between ratio of Ga/Mg and V, see Figure 47. Rubies from Cambodian-Thai had higher Mg and therefore lower ratio of Ga/Mg which can separate from other localities. Mozambique rubies contained lower V than rubies from Madagascar and Cambodian-Thai. However, Winza presented lowest V content or below detection limit whereas Vatomandry contained highest V up to 83 ppma which corresponded to results from Schwarz, 2001.

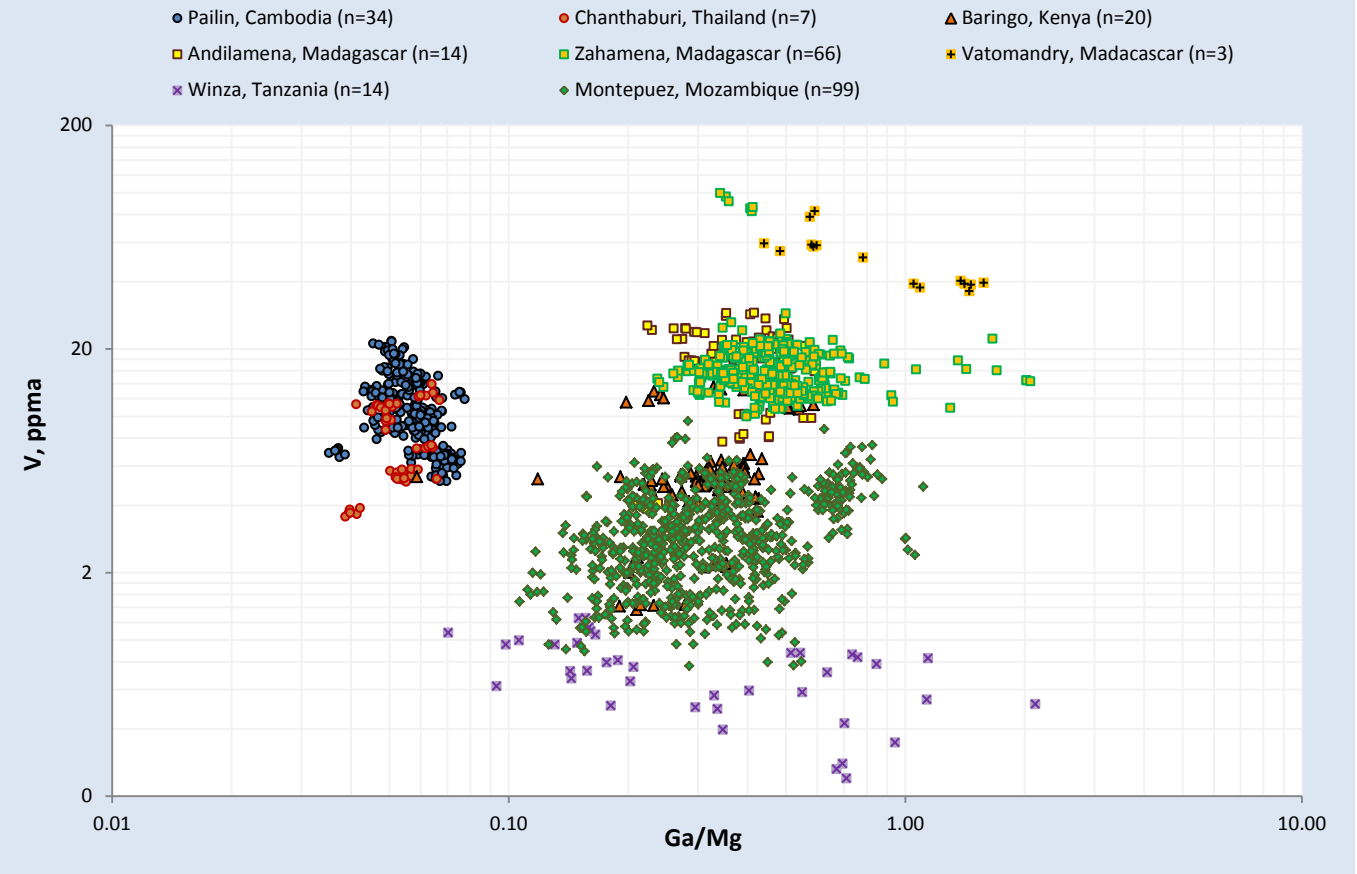

Figure 47: Plot of Ga/Mg versus V in ppma for different localities.

Table 6: Some elemental composition in rubies from six different geographical localities using LAICPMS [Min-Max range (average±SD)]* in ppma or parts per million by atom.

Element	Pailin, Cambodia (n=34 , 272spots)	Chanthaburi, Thailand (n=7, 54spots)	Montepuez, Mozambique (n=85, 554spots)	Andilamena, Madagascar (n=14, 84 spots)	Zahamena, Madagascar (n=66, 318 spots)	Vatomandry, Madacascar (n=3, 15spots)	Winza, Tanzania (n=20, 59spots)	Baringo, Kenya (n=20, 108spots)	Detection limit
^{24}Mg	97-258 (154±28)	126-181 (143±13)	8-65 (28±11)	19-53 (36±7)	13-61 (35±8)	9-43 (24±12)	BDL-118 (22±21)	BDL-159 (27±19)	0.17
^{47}Ti	32-138 (77±26)	36-89 (54±15)	BDL-59 (21±9)	14-54 (34±8)	8-113 (35±11)	16-79 (36±20)	BDL-82 (14±20)	4-49 (17±8)	0.94
^{51}V	5-22 (11±4)	4-14 (8±3)	BDL-10 (3±1)	4-29 (18±7)	10-100 (17±11)	36-83 (51±15)	BDL-1 (0.5±0.4)	1-14 (6±3)	0.093
^{53}Cr	162-2494 (979±497)	859-1945 (1295±249)	185-4941 (1317±872)	53-1569 (403±377)	135-3922 (1196±874)	737-1342 (1010±225)	161-1094 (583±295)	335-1212 (594±165)	0.63
^{57}Fe	818-1935 (1317±252)	756-1442 (1089±247)	231-2514 (843±550)	559-1559 (1009±253)	284-1994 (912±249)	517-966 (782±133)	405-1596 (817±276)	337-767 (548±100)	2.18
^{60}Ni	0.8-7 (3±1)	2-4 (3±1)	BDL-1 (0.2±0.2)	BDL-0.4 (0.1±0.1)	BDL-0.6 (0.1±0.1)	0.9-3 (2±0.9)	BDL-4 (0.3±0.7)	BDL	0.05
^{69}Ga	5-11 (9±1)	5-10 (8±1)	5-14 (8±2)	7-21 (14±4)	10-30 (16±4)	13-22 (18±3)	4-11 (6±1)	7-13 (9±2)	0.06

*Data reported in minimum and maximum values, with average and standard deviation in parentheses; BDL = below detection limit

PART IV. SUMMARY

The border Trat-Pailin area has been an active ruby mining for over 100 years. In the second half of the 20th century, the area was a main supplier of ruby. This increased production was necessary to feed the Thai jewelry industry after the supply of Burmese ruby was cut off. Although mining of Thai rubies is neglectible nowadays, ruby mining around Pailin is continuing. The scale of the mining is much smaller than 40 years ago, but good material is still being mined. The gemstone deposits on the Thai-Cambodian border are related to alkali-basalts. These mafic rocks formed deep in the earth and picked up the corundum on its way to the surface. The rubies (and sapphires) did not form in these basalts, thus they should be called xenocrysts. The amount of gem corundum in the total volume of basalt is very low, but most minerals in the basalt (pyroxenes) are unstable and weather easily in the conditions present on the surface in Southeast Asia. The gem corundum can be found in reddish mud (colluvial) or in gravels where they are concentrated by moving water (alluvial). Almost all of the ruby mining is done in the deposits related to the rivers. In Cambodia, miners are working in older, buried riverchannels and in the active riverbed. The scale of the mining varies from artisanal handwork in the rivers to larger mechanized operations.

Cambodia-Thai rubies have distinct inclusions such as crystals associated with decrepitation haloes in basal planes, lamellar twinning with intersecting growth tubes and naturally fluid fingerprints with hexagonal haloes. . Only Baringo, Kenya rubies contained thin film like inclusions which similar to Cambodia-Thai rubies, but there are significant differences in chemistry. There are no rutile needles observed in Thai/Cambodia rubies unlike those rubies from Mozambique, Winza (Tanzania), Zahamena and Vatomandry (Madagascar).

UV-Vis-NIR spectra of Cambodia-Thai rubies show a combination of chromium and iron chromophores. The iron spectrum is dominating when chromium content is low. Every studied sample shows a high background absorption starting from 600 nm into the ultraviolet (UV) region. This absorption feature is the characteristic of natural rubies caused by Fe^{2+}-Ti^{4+} charge transfer absorption spectrum. Due to the significantly chromium spectrum, the Fe^{2+}-Ti^{4+} charge transfer peak at 580 nm is hidden. Fe^{2+}-Ti^{4+} charge transfer spectrum is shown pure chromium spectrum is subtracted from the total spectrum. However, it only slightly contributes to the color in rubies from Cambodian-Thai border region resulting in purplish red. FTIR spectra obtained from Cambodian-Thai rubies in the mid to infrared region ranging from 1500 to 5000 cm^{-1} were not diagnostic or very slightly single 3309 cm^{-1} and Kaolinite mineral. Population plotting between Ga/Mg and V are the most useful for origin determination, especially when stones are lacking inclusions or when stones are heated at high temperature which is commonly done with Cambodia-Thai rubies to lighten a dark color or remove a blue tint. The presence of Ni can also be used to separate these gems from other high Fe rubies.

This article provides new data, collected to the standards of a modern gemological laboratory, on Cambodian-Thai rubies. Although these gems are no longer being actively mined on an industrial scale, they are historically one of the most important ruby sources.

ACKNOWLEDGEMENTS. The authors acknowledge and thank Dr. John Emmett for useful advice and support. We also thank Jonathan Muyal, Charuwan Khowpong and Victoria Raynaud-Flattot for the microphotographs. The chemical analysis was performed by Ungkhana Atikarnsakul and Vararut Weeramonkhonlert. Yunbin Guan is thanked for his assistance with the SIMS-analysis at Caltech,CA.

ABOUT THE AUTHORS. Dr. Supharart Sangsawong is a former research scientist from GIA, currently working as gemstone testing manager at the Bahrain Institute for Pearls & Gemstones (Danat). Wim Vertriest (wvertrie@gia.edu) is field gemologist at GIA's Bangkok laboratory. Sudarat Saeseaw (ssaeseaw@gia.edu) is senior manager of colored stone identification in GIA's Bangkok laboratory. Vincent Pardieu (vince@fieldgemology.org) is the former senior manager of GIA's field gemology department, currently working as an independent consultant at 'VP Consulting'.

PART V. BIBLIOGRAPHY

Beran, A., and Rossman, G. R. (2006). OH in naturally occurring corundum. *European Journal of Mineralogy*, 18 (4), 441-447.

Emmett, J.L., Stone-Sundberg, J., Guan, Y., andSun, Z. (2017). The role of silicon in the color of gem corundum. *Gems & Gemology*, 53(1), 42-47.

Ferguson, J., and P. E. Fielding (1971). The origins of the colours of yellow, green and blue sapphires, *Chemical Physics Letters*, 10(3), 262-265.

Jobbins, E.A., F.I.M.M., Berrange J.P. (1981). The Pailin ruby and sapphire gemfield, Cambodia. *Journal of gemology*. Vol17, no8, pp555-567.

Keller, P.C. (1982).The Chanthaburi-Trat Gem Field, Thailand. *Gems & Gemology*, 18(4): 186-196.

Gübelin, E.J., and Koivula, J. I. (1986), Photoatlas of Inclusions in Gemstones Vol.3. Opinio Publisher, Basel, Switzerland.

Gübelin, E.J., New analytical results of the inclusions in Siam rubies. *Journal of gemmology*. Vol12. No7. p242-252.

Hänni, H., and K. Schmetzer (1991), New rubies from the Morogoro area, Tanzania, Gems & Gemology, 27(3), 156-167.

Hughes R. W., Manorotkul W. and Hughes E.B. (2017), Ruby and sapphire: a gemologist's guide, 1st edition, RWH Publishing/Lotus Publishing, Thailand. Chapter 4.

Hughes, R. W. (1996). "Death of the Thai ruby." JewelSiam(August/September): 100-105.

Levinson, A. A. and F. A. Cook (1994). "Gem corundum in alkali basalt: Origin and occurrence." Gems & Gemology, 30 (4), pp. 253–262.

Moon, A.R. and Phillips, M.R. (1994) Defect clustering and colour in Fe, Ti: α-Al2O3. *Journal of the American Ceramic Society*, Vol. 77, No. 2, pp. 356–367; RWHL

Nassau, K. (1978). The origins of color in minerals, *American Mineralogist*, 63(3-4), 219-229.

Pardieu, V., T. Jitlapit, J. Stephane, S. J. Baptiste, B. L. Pierre. Rubies from the Niassa and Cabo Delgado regions of Northern Mozambique. GIA News from Research. https://www.gia.edu/gia-rubies-from-niassa-cabo-delgado

Pardieu, V., Sangsawong, S., Muyal, J., Chauviré, B., Massi, L., and Sturman, N. (2013), MONTEPUEZ AREA (MOZAMBIQUE), GIA News from Research. https://www.gia.edu/gia-rubies-from-montepuez-area

Pardieu, R. W. H. V. (2009). Red Sky at Dusk: Hunting the Last Siamese Ruby Miner.

Powell, R.C. (1998). Physics of Solid-State Laser Materials. New York, Springer-Verlag, 423 pp.

Ridd, M. F., Barber, A.J., Crow, M.J. (2011). The Geology of Thailand.

Schwarz, D., et al. (2008), Rubies and sapphires from Winza, central Tanzania, *Gems & Gemology*, 44(4), 322-347.

Schwarz, D., and K. Schmetzer (2001), Rubies from the Vatomandry area, eastern Madagascar, *Journal of gemmology*, 27(7), 409-416.

Sutherland, F. L., D. Schwarz, E. A. Jobbins, R. R. Coenraads, and G. Webb (1998), Distinctive gem corundum suites from discrete basalt fields: A comparative study of Barrington, Australia, and West Pailin, Cambodia, gemfields, *Journal of Gemmology*, 26(2), 65-85.

Sutherland, F. L., Hoskin, P.W.O., Fanning, C.M., Coenraads, R.R., (1998). "Models of corundum origin from alkali basaltic terrains, a reappraisal." Contrib Mineral Petrol (133): pp.356-372.

Saminpanya, S., Manning, D.A.C., Droop, G.T.R., Henderson, C.M.B. (2003). Trace elements in Thai gem corundums. Journal of gemmology, 28, 399-415.

Saminpanya, S., Sutherland, F.L., (2011). "Different origins of Thai area sapphire and ruby, derived from mineral inclusions and co-existing minerals." Eur. J. Mineral. **23**: pp. 683–694.

T. Thomas. Corundum C-Axis Device for Sample Preparation. Research News (2009). https://www.gia.edu/gia-news-research-nr6809